Journal of Materials Chemistry A

Accepted Manuscript

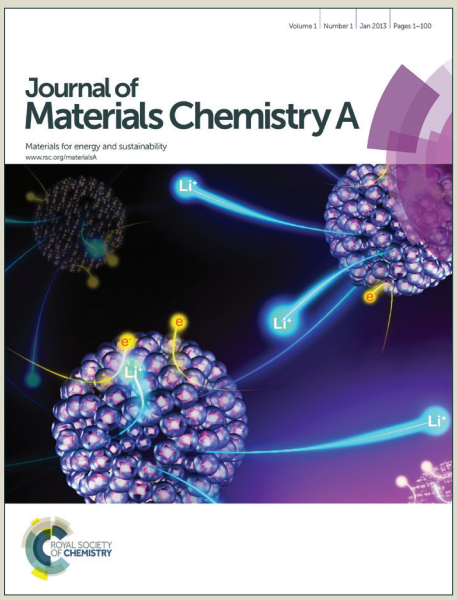

ROYAL SOCIETY OF CHEMISTRY

www.rsc.org/materialsA

Journal Name

RSCPublishing

ARTICLE

Microfibrillated cellulose reinforced bio-based poly(propylene carbonate) with dual shape memory and self-healing properties

Cite this: DOI: 10.1039/xoxxoooooox

Received ooth January 2012,
Accepted ooth January 2012

DOI: 10.1039/xoxxoooooox

www.rsc.org/

Xiaodong Qi,[a] Guanghui Yang,[a] Mengfan Jing,[a] Qiang Fu[*a] and Fang-Chyou Chiu[*b]

A novel biological friendly shape memory polymer and self-healing polymer based on poly(propylene carbonate) (PPC)/microfibrillated cellulose (MFC) was prepared. MFC was firstly modified by a one-step mechanic-chemical approach involves ball milling and esterification reaction. In this way MFC could be incorporated into PPC up to 20 wt% with excellent dispersion. The formation of "MFC network" structure in the PPC matrix was verified via scanning electron microscopic and the strong interfacial interaction between PPC and MFC was confirmed by X-ray photoelectron spectroscopy. The incorporation of MFC not only significantly enhanced mechanical strength and thermal stability, but also acted as physical cross-linkers, which could improve the shape memory property of PPC at definite content (5~10 wt%). More importantly, with the assistance of shape memory effect and the reinforcement of MFC fibers, the polymer composites also showed much enhanced scratch resistance and scratch self-healing behavior. Our work provides a composite approach to tune the shape memory behaviors of polymer composites and may contribute to the application of PPC in smart materials field.

1. Introduction

Smart polymer materials such as shape memory polymers (SMPs) and self-healing polymers (SHPs) can sense and respond to the external stimuli such as heat, light, electricity, magnetic field and humidity.[1-6] Therein, SMPs possess the ability to undergo a large recoverable deformation when subjected to external stimuli. For another one, SHPs have the capability to self-repair from a physical damage upon the application of an external stimulus. These two features are both amazing properties which can greatly widen the materials' applications.

SMPs typically consist of two elements: molecular switches and netpoints.[7] The molecular switches are polymer chains incorporated into the network, which are responsible for the shape memory cycle. Netpoints are typically the connection points for polymer chains in a network and determine the permanent shape. Normally, SMPs should contain a finite content of chemical cross-linkers to form a "memorable" network or possess some degree of hard regions as physical cross-linkers. This broad view is supported by a number of examples of SMP that introducing high content of nanoparticles in polymers to act as cross-linkers.[8-16] For example, utilizing a coagulation spinning process, Miaudet fabricated polyvinyl alcohol nanocomposite fibers consisting of 20 wt% carbon nanotubes.[8, 9] The fibers exhibited shape memory behavior despite the fact that they did not fit the typical profile of SMPs. Dong investigated shape memory behavior of poly(acrylamide-co-acrylic acid) grafted on graphene.[10] Graphene, which could control the motion of polymeric chains, served as physical cross-linkers and endowed the nanocomposites with shape memory properties. According to previous studies, for SMPs that introducing nanoparticles as netpoints, two concerns are needed to take into consideration.[17] One is the strong interactions between polymer chains and fillers; the other is fully cross-linked netpoints, which often needs high content fillers. To do this, it's necessary to better design matrix-filler interactions and filler-filler interactions as well.

On the other hand, the development of materials that exhibiting shape memory assisted self-healing property is of interest as the shape memory behavior can be used to aid the healing process by bringing fractured surfaces into close proximity, allowing them to be more efficiently healed.[3, 18-22] For instance, Rown reported a structurally dynamic polydisulfide network which could exhibit both shape memory and healable properties.[18] Zhao also investigated the improved self-healing property of cross-linked polyethylene/carbon black nanocomposites by shape memory effect (SME).[19] However, a scratch often leads to crack, which may be irreparable via the reverse plasticity SME.[22] One possible solution is to enhance the crack

resistance of SMPs so that cracks are difficult to form in a scratching situation. This can be solved by SMPs employing inorganic nanoparticles as netpoints due to their improved mechanical properties.

In view of better sustainability, development of new SMPs or SHPs derived from biomass is highly desired, especially for biomedical fields. To the best of our knowledge, a relatively few work has been reported on the SMPs or SHPs derived from nonpetro-chemical feedstock.[11, 23] Poly(propylene carbonate) (PPC), as a new biomaterial, is produced via polymerization of propylene oxide and carbon dioxide, and attracts considerable attention, not only due to its high value-added fixation of CO_2 as an efficient route to reduce gas pollutions and overcome shortages in petroleum, but also due to its biodegradability and biocompatibility.[24, 25] However, its low mechanical strength, poor thermal stability severely limit its practical application. In previous studies, several fillers including graphene oxide, montmorillonite and clay have been incorporated into PPC to enhance the mechanical performances and thermal stability.[26-28] Nevertheless, the harm of these non-biodegradable fillers on human still remains debatable, so new biodegradable fillers are needed to prepare environmental friendly PPC composites.

Microfibrillated cellulose (MFC) has become topic of interest in polymer modification owing to its low density, high aspect ratio (ca. 10 nm in diameter and 300~500 μm in length), excellent mechanical properties, relatively reactive surface, readily biocompatibility and biodegradability.[29] These characters have led MFC to be excellent filler for the enhancement of polymer composites, especially for biodegradable polymers to prepare full biodegradable composites. So far, studies have mainly focused on polymer composites at a rather low MFC content (usually below 5 wt%).[29-31] It is a great challenge for preparing composites with high content MFC due to the easy aggregation of MFC. The key to prepare uniformly dispersed MFC in polymer matrix are to effectively avoid the aggregation of MFC (disentanglement) and enhance the interactions between polymer chains and MFC.

In this work, in order to improve the low mechanical strength and poor thermal stability of PPC composites with good biodegradability and biocompatibility, also with good shape memory and self-healing properties, a simple one-step mechanic-chemical approach was firstly applied to modify MFC and disentangle MFC simultaneously. Then a high content (up to 20 wt%) of MFC was incorporated into PPC to prepare PPC/MFC composites. The dispersion and interaction of MFC and PPC were verified via scanning electron microscope and X-ray photoelectron spectroscopy. The prepared composites exhibited excellent high mechanical strength at both room temperature and high temperature (above the glass transition temperature (Tg) of PPC). Moreover, with the enhancement of MFC, PPC/MFC composites displayed significant property improvement over the neat PPC including shape memory property, scratch resistance and thermal healing capability.

2. Materials and methods

2.1 Materials

Poly(propylene carbonate) (PPC) powders were supplied by Changchun Institute of Applied Chemistry, Chinese Academy of Science (Jilin, China). Its weight-average molecular weight (M_w) was 2.48×10^5 g mol^{-1} and M_w/M_n was 3.2. Microfibrillated cellulose (Celish MFC KY100-S) was purchased from Daicel Chemical Industries, Ltd. (Japan). N,N-dimethylformamide (DMF) supplied by Tianjin bodi chemical Co. Ltd. was dehydrated before using. Acetyl chloride (AC) was obtained from Tianjin bodi chemical Co. Ltd. and used as received.

2.2 Preparation of modified microfibrillated cellulose nanofibers

MFC was modified by a one-step mechanic-chemical approach involves ball milling of cellulose in DMF containing an esterifying agent, aimed at improving the dispersion of MFC in hydrophobic media.[32] We chose acetyl chloride which was more accessible rather than hexanoyl chloride as the esterifying agent. In brief, MFC was firstly dried in vacuum at 70 ^oC until its weight unchanged. Then 0.5 g MFC was added to 100 ml DMF under vigorous magnetic stirring for 12 h. After that, the impregnated MFC was homogenized in DMF via the high-shear mulser (FA25, Shanghai Sumai Trading Co., Ltd.) at 15000 rpm for 1 h (15 min pause after every 10 min to prevent overheating). Then 50 ml homogenized MFC/DMF solution (4.6 mg mL^{-1}) and 4 ml AC were added in four dried 100 ml zirconia cylinders loaded with zirconia balls (10 mm diameter) of the planetary ball mill (QM-3SP2, Nanjing University Instruments Plant). Mill was driven at 500 rpm under programmed punctuated operation (10 min pause after every 40 min, alternate between turning and reverse) for 8 h. The reaction mixture was cleaned by centrifugation to remove the acid and impurity followed by ultrasonication for 30 min to produce well-dispersed MFC in DMF. Hereinafter, the obtained MFC through the mechanic-chemical approach are denoted as MFC-BR (modified by ball milling and reaction). For comparison, the homogenized MFC/DMF solution modified by ball milling without AC and the solution modified by esterifying (reaction with AC) without ball milling were also prepared, denoted as MFC-B (modified by ball milling individually) and MFC-R (modified by esterifying individually) respectively.

2.3 Preparation of PPC/MFC composites

2 g PPC was dissolved in 20 ml DMF under vigorous stirring to yield a clear solution. Then a certain amount of MFC-BR/DMF solution was added into the PPC/DMF solution under vigorous stirring for 2 h. After that, the homogeneous PPC/MFC-BR/DMF solution was poured into glass frames. The casting films were dried in an air-circulating oven at 70 ^oC to remove DMF quickly and then dried in a vacuum oven at 60 ^oC for 48 h. The obtained PPC/MFC-BR composites contained 0 wt%, 5 wt%, 10 wt%, 15 wt%, 20 wt% MFC-BR are denoted as PPC, PPC5, PPC10, PPC15, PPC20, respectively.

2.4 Characterization

Fourier transform infrared spectroscopy (FTIR) measurements were performed on a Thermo Scientific Nicolet 6700 spectrometer (Thermo Electron Corporation) equipped with an attenuated total reflection (ATR) accessory.

The chemical composition of elements was analyzed by X-ray photoelectron spectroscopy (XPS, Axis Ultra DLD, Kratos Co., UK) using focused monochromatized Al Ka radiation (15 kV).

To observe the morphology of fillers, MCF, MFC-BR, MFC-B and MFC-R were firstly spin coated on mica plates, and then the plates were dried and coated with gold for scanning electron microscope (SEM) analysis. To observe the dispersion of MFC-BR

in PPC, the cross-section was exposed by fracturing the composites in liquid nitrogen and then the surface were etched in a mixed solution of anhydrous ethanol and acetone (1/1, v/v) at room temperature for 30 min to partially remove PPC. All these samples were observed using an Inspect field-emission SEM (FEI Company, USA) with 5 kV accelerating voltage.

Tensile properties of PPC and PPC/MFC-BR composites at room temperature (23 °C) were measured using an Instron 5567 universal testing machine with a crosshead speed of 20 mm/min. The tensile tests at 60 °C were performed on a Q800 dynamic mechanical analyzer (DMA, TA Instruments). Uniform rectangular specimens of 20 mm × 2 mm × 0.5 mm were loaded with a controlled ramp rate of 3 N min^{-1}. In order to ensure accuracy, at least three specimens of each sample were tested.

The impacts of MFC on the dynamic mechanical behavior of PPC were evaluated under a tension mode on a Q800 DMA (TA Instruments). A frequency of 1 Hz and an amplitude of 10 μm were employed. The temperature ranged from -10 °C to 100 °C at a heating rate of 3 °C min^{-1}.

The thermal stability of the composites was evaluated by thermo gravimetric analysis (TGA Q500, TA instrument). It was performed by heating the specimens (1~10 mg) from 50 °C to 500 °C at a heating rate of 10 °C min^{-1} in nitrogen flow.

To investigate the shape memory behavior, a four-step program was used on DMA as follows; (1) Deforming, the sample was stretched to a strain (ε_m) with a constant force at 60 °C. (2) Fixing, the sample was then cooled to low temperature (25 °C) under a constant force. (3) Unloading, the external force was removed and then recorded the strain (ε_u). (4) Recovery, the sample was reheated to 60 °C to observe the recovery process and recorded the strain (ε_p). Shape recovery ratio (R_r) and shape fixing ratio (R_f) were evaluated according to formula (1) and (2).

$$R_r = \frac{\varepsilon_m - \varepsilon_p}{\varepsilon_m} \quad (1)$$

$$R_f = \frac{\varepsilon_u}{\varepsilon_m} \quad (2)$$

Self-healing tests. The prepared films with width of 0.5 mm were stretched by an ε of 50 % on a hot stage at 60 °C and then quickly cooled to room temperature under the force. Then the force was removed and a sharp blade was used to make a straight scratch in the direction perpendicular to the previous stretching direction. To confirm shape memory assisted self-healing effect, control tensile test experiment with scratch but without stretching was also carried out. The self-healing process was observed by an optical microscope with a heating platform and the whole healing process from room temperature to 60 °C with a rate of 5 °C min^{-1} was recorded by a camera. Considering the small space of the heating platform in optical microscope, the specimen was cut into 20 mm × 2 mm × 0.5 mm, which is more suitable for DMA measurement. The tensile test was performed on a Q800 dynamic mechanical analyzer (DMA, TA Instruments). Uniform rectangular specimens of 20 mm × 2 mm × 0.5 mm were loaded with a preload of 0.001N and a controlled ramp rate of 3 N min^{-1} ranged from 0 N to 18 N.

3. Results and discussions

3.1 Modification and characterization of MFC

MFC is a kind of bio-based material with high aspect ratio and plenty of hydroxyl groups. Therefore, MFC is easy to be aggregated due to the intermolecular forces (such as hydrogen bonds) and physical interactions (such as entanglements) among the fibers. It is necessary to modify MFC to improve its dispersion in organic solvents before the preparation of PPC/MFC composites with high content filler. Hence, MFC was firstly modified by a one-step mechanic-chemical approach in our work. During this procedure, on the one hand, MFC could be physically exfoliated by the shear force caused from the rigid milling balls; on the other hand, the esterification reaction between the hydroxyl groups on the surface of MFC and highly reactive acetyl chloride could take place in the ball milling cylinders. Thus some of the hydroxyl groups of MFC can be replaced by acetyl groups, which could reduce the interactions (hydrogen bonds) among MFC and improve its dispersion in organic solvents. In order to verify the effectiveness of this modification, FTIR and SEM were performed and discussed in the following part.

The evidence of the covalent bonding between MFC and AC is provided by FTIR spectra. As shown in Fig. 1, compared with MFC, after the mechanic-chemical modification procedure, the O-H stretching peak (3340 cm^{-1}) is weakened and two absorption peaks at about 1730 cm^{-1}, 1226 cm^{-1} are distinctly observed in the spectrum of MFC-BR. They are corresponded to the stretching vibration of the carbonyl groups (C=O) and the C-O of ester groups (-COO-), demonstrating that the esterification reaction has occurred between hydroxyl groups and AC. These absorption peaks suggest the existence of hydroxyl and carbonyl groups on the surface of MFC, which could provide the active centers for the blend with PPC.

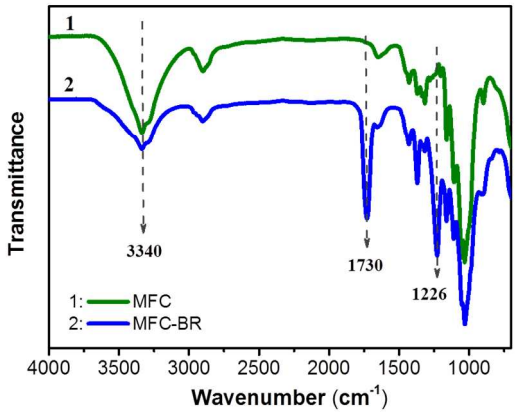

Fig. 1 The FTIR spectra of MFC and MFC-BR.

Fig. 2 presents the SEM images of MFC, MFC-R, MFC-B and MFC-BR, respectively. As shown in Fig. 2a, MFC fibers are dispersed as agglomerates in micron scale. It is found that the size of MFC-R (Fig. 2b) and MFC-B (Fig. 2c) agglomerates become much smaller compared with raw MFC. However, the diameter of MFC-R or MFC-B is still large and the entanglement among the fibers is seriously. So it is not efficient enough to improve the dispersion of MFC by using a mechanical or chemical method individually. In Fig. 2d, the size of MFC-BR fibers is seen to be the smallest among the samples, and can be less than 100 nm for some fibers. More

importantly, MFC fibers are mostly exfoliated into single fibers and can be individually dispersed in the solution or on mica plates. Thus, the approach by using mechanical and chemical methods simultaneously has synergetic effect in achieving excellent dispersion of MFC. Based on this result, MFC-BR is expected to add into PPC with good dispersion, particularly for high content fillers.

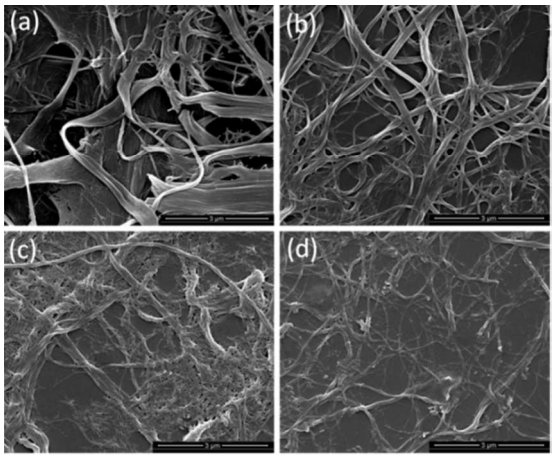

Fig. 2 SEM of MFC (a), MFC-R (b), MFC-B (c) and MFC-BR (d).

3.2 Dispersion morphology of MFC in composites

To observe the dispersion state of MFC-BR in the PPC matrix, SEM is performed and the result is shown in Fig. 3. Compared with the smooth surface of neat PPC (Fig. 3a), all composites present typical crumpled morphology and become more pronounced with the increase of MFC-BR content. This is mainly ascribed to the different structures and stiffness between polymer matrix and fillers.[33] It can be seen that MFC-BR is distributed homogeneously in PPC matrix without obvious aggregation when the content of MFC-BR is 5 wt% (Fig. 3b). With the MFC-BR content increases from 5 wt% to 10 wt%, the packing density of MFC-BR increases gradually and some fibers become to agglomerate in the PPC matrix, forming a network-like structure (Fig. 3c). MFC-BR is one-dimensional filler with high aspect ratio and it is easy to be entangled with each other at high content. When the content of MFC-BR is as high as 20 wt%, a more compact distribution of MFC-BR is observed (Fig. 3d). In this case, MFC-BR network is clearly observed. It is believed that the filler morphology can significantly restrict the mobility of PPC chains.

In order to better analyze the network structure formed by MFC fibers at higher content, the surfaces of PPC10 and PPC20 were etched in a mixed solution of anhydrous ethanol with acetone (1/1, v/v) to partially remove PPC and better exposed MFC fibers were shown in Fig. 3 (e, f). It is clearly seen that the MFC-BR fibers are almost mono-dispersed in nanoscale throughout the PPC matrix. And these fibers are interpenetrated each other and a "MFC-BR network" structure seems to form in the PPC matrix. The globular materials are the residual PPC after etching. The formation of filler network is usually observed in polymer nanocomposites and can be further verified via rheological method.[34] Unfortunately, PPC is easily degraded at high temperature and we fail to use rheological method or transmission electron microscope to further confirm the formation of MFC network in the prepared composites.

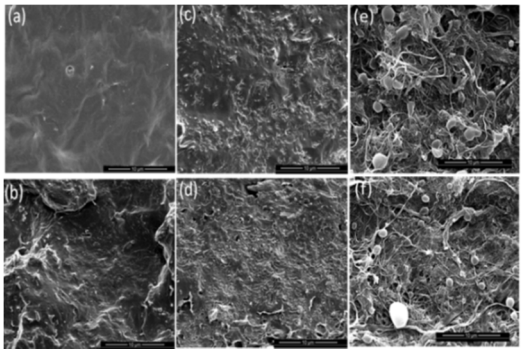

Fig. 3 Fractured surface of PPC (a), PPC5 (b), PPC10 (c), PPC20 (d) and etched surface of PPC10 (e), PPC20 (f).

3.3 Analysis of filler–polymer interactions

The good dispersion of MFC-BR in PPC at high filler content implies sufficient interfacial adhesion between the filler and polymer matrix. X-ray photoelectron spectroscopy (XPS) is known for its remarkably higher sensitivity and selectivity, when applied to analyze non-covalent filler-matrix interactions in polymer composites.[12, 35] Thus XPS was carried out to examine the possible interactions between MFC-BR and PPC, and the obtained spectra are shown in Fig. 4. It is observed that the O 1s binding energy of the C=O groups and C-O groups from PPC are shifted to lower value because of the electron transfer to the hydroxyl and carbonyl groups of MFC. Specifically, the PPC chain contains C=O and C-O groups that can participate in various interactions (C=O---H-O, C=O---O=C, C=O---O-C) with the oxygenated functional groups of MFC-BR. While these non-covalent interactions are individually weak, their collective contribution can be quite significant. As a result, MFC-BR combines with PPC through sufficient interactions, contributing to the good dispersion of MFC-BR and the mechanical reinforcement of PPC as shown below.

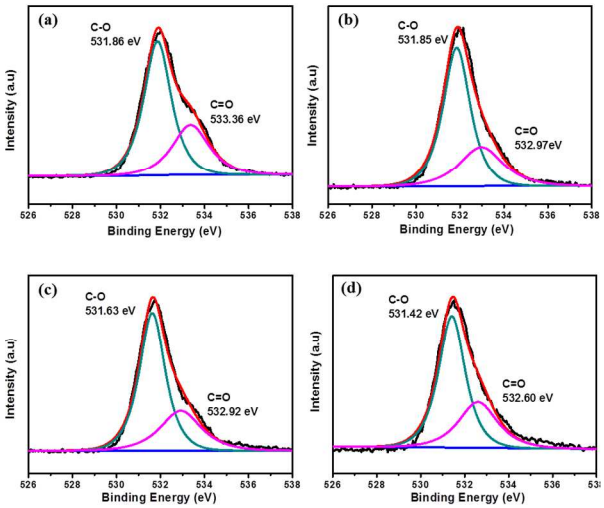

Fig. 4 XPS (O1s) of neat PPC and PPC/MFC-BR composites, (a)PPC, (b)PPC5, (c)PPC10, (d)PPC20.

3.4 Mechanical properties of the PPC/MFC-BR composites

It is known that the poor high-temperature mechanical properties restrict the practical application of PPC. Even a small increase in

temperature will make the completely amorphous PPC change from a glassy state to a rubbery state, which directly leads to a drastic drop of mechanical properties. In this study, we expect to enhance the high-temperature mechanical properties of PPC through a formation of MFC-BR network. Fortunately, via a one-step mechanic-chemical modification of MFC and a solution casting method, we have successfully prepared PPC/MFC-BR composites with good dispersion even at a high content of MFC-BR. Then we studied the mechanical properties of the obtained composites. Two representative temperatures are considered for the tensile testing, 23 ^{o}C (room temperature) and 60 ^{o}C (above the Tg of PPC).

At room temperature (Fig. 5a), the tensile strength of PPC sharply increases from about 2 MPa to 25 MPa after incorporating 5 wt% MFC-BR. By adding 10 wt% MFC-BR, the tensile strength increases to 45 MPa. The dramatic increase in mechanical properties is mainly attributed to the high mechanical stiffness of MFC-BR, as well as the good dispersion and strong interactions between MFC-BR and PPC. Moreover, with further increase of MFC-BR content to 15 wt% or 20 wt%, only a slight increase in tensile strength is observed, indicating a saturated phaenomenon, as reported in other polymer composites.[10, 33]

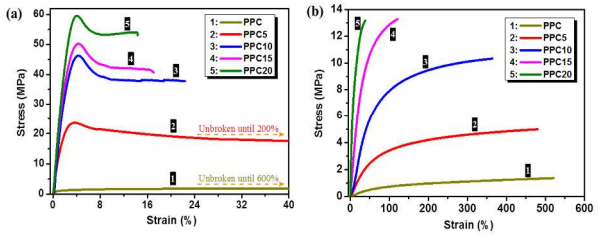

Fig. 5 Tensile behaviors of neat PPC and PPC/MFC-BR composites. Stress-strain curves versus the content of MFC at room temperature (a) and 60 ^{o}C (b).

It is also of great importance to evaluate the tensile properties of composites at T > Tg because an external force will be loaded to accomplish its temporary shape for shape memory experiments.[36] Thus the tensile testing is carried out at 60 ^{o}C with DMA and the result is shown in Fig. 5b. The tensile strength of neat PPC becomes only 1 MPa at such a high temperature. The chains of PPC are in rubbery state and can be easily removed by external force, resulting in lower mechanical strength but much enhanced elongation than that at room temperature. As for PPC5 and PPC10, the tensile strength increases to 4 MPa and 10 MPa, combined with a decreased elongation. With the increase of MFC-BR content over 10 wt%, the tensile strength is further improved to 13 MPa for PPC15 and PPC 20, but the elongation is dropped to 100% or even less. It should be noted that the tensile strength and elongation achieved at 60 ^{o}C for PPC10 and PPC15 are better than those of some traditional polymers such as polypropylene (PP) or polylactic acid (PLA), as shown in Table 1.[37, 38] Therefore, PPC/MFC-BR composites prepared in this study exhibit a potential to be used as an alternative material to traditional polymers at high temperature.

Table. 1 A comparison study of average mechanical properties of PPC10, PPC15, PP, and PLA at around 60 ^{o}C.

Sample	Tensile strength (MPa)	Strain at break (%)	Ref
PPC10	10.8±0.4	360±25	
PPC15	13.2±0.7	121±12	
PP3371	17.2	9.19	[37]
PLA	8	2	[38]

3.5 Dynamic mechanical analysis

DMA was carried out to study the thermal mechanical properties of the PPC composites. From Fig. 6a, the storage modulus of the prepared composites increases significantly with the increase of MFC-BR content. Moreover, as the content of MFC-BR increases to 10 wt%, the storage modulus tends to shift to high temperature obviously, and the loss modulus peaks present similar trends (Fig. 6c), indicating a sharp increase of the Tg (from 27 ^{o}C to 39 ^{o}C). The increase of storage modulus and Tg could be attributed to the enhancement of the combined effect caused by the rigid MFC-BR fibers, and the strong interactions between PPC and MFC-BR. As the content of MFC-BR increases to over 10 wt%, the storage modulus still shows an obvious increase while the Tg keeps relatively constant. Interestingly, as shown in Fig. 6b, although all the composites show sharply decline in storage modulus when the temperature is higher than the Tg of PPC, the decline becomes smaller with the increase of the MFC-BR content. For instance, the storage modulus of PPC decreases to near zero at 60 ^{o}C while it can still remain at about 300 MPa and 500 MPa for PPC15 and PPC20. This phenomenon illustrates that there exists a stiff continuous structure to bear the external forces loaded on the PPC/MFC-BR composites with high content fillers. According to the SEM analysis above, the stiff continuous phase can only be the MFC-BR network.

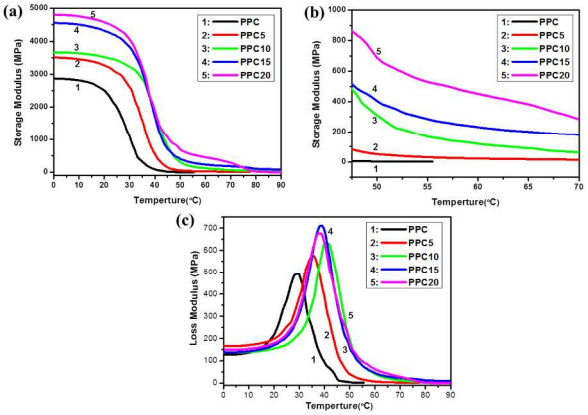

Fig. 6 DMA of neat PPC and PPC/MFC-BR composites. (a) Storage modulus as a function of temperature. (b) The magnification of curves in the temperature range of 45-70 ^{o}C. (c) Loss modulus as a function of temperature.

3.6 Thermal stability

TGA measurement was performed to study the thermal stability of the obtained composites. As shown in Fig. 7a, the initial thermal decomposition temperature of PPC increases from 130 ^{o}C to about 180 ^{o}C because of the incorporation of MFC-BR. Fig. 7b shows a more remarkable improvement of the maximum decomposition temperature with the increase of MFC-BR content. For instance, the maximum decomposition temperature increases sharply from 234 ^{o}C to 268 ^{o}C by incorporating 10 wt% MFC-BR. When the fillers

content is as high as 20 wt%, an increase of 60 °C in the maximum decomposition temperature is realized. This demonstrates that MFC-BR can effectively prevent heat transfer in the PPC/MFC-BR composites, resulting in the improvement of the heat resistant properties of PPC.

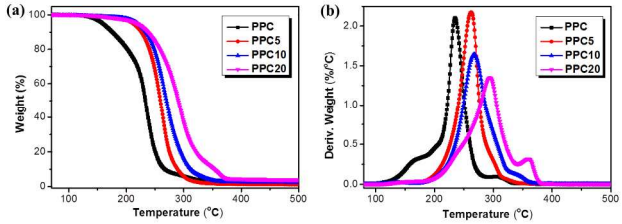

Fig. 7 TGA curves of PPC and PPC/MFC-BR composites.

3.7 Shape memory properties

Previous studies suggest that ensuring fully cross-linked netpoints those are uniformly distributed is the key factor for achieving completely recovery.[17, 23] In our work, the large surface area of MFC-BR and its high weight fraction ensure a high fraction of interfacial zone within which the molecular mobility is hindered by the strong interactions between PPC and MFC-BR. Thus, it's presumed that MFC-BR fibers would enhance the shape memory property of PPC. Fig. 8 shows shape memory behavior of PPC and PPC/MFC-BR composites. The fix ratio (R_f) and recovery ratio (R_r) measured by cyclic thermomechanical tensile tests were given in Table 2. There is poor shape memory ability for the pure PPC. With the content of MFC-BR increasing to 10 wt%, R_f and R_r both increase to nearly 95%. The shape can recover well when the content of MFC-BR is as high as 10 wt% (Fig. 8 (b, c)). As an example, Fig. 9 shows two groups about the stretched strip of PPC5 can recover to the original shape in 30 s when heated at 60 °C. The MFC-BR fibers, which serve as physical cross-linking points, retard chain relaxation and augment the amount of frozen strain during loading and cooling.[39] This is especially true for cross-linked SMPs, where less relaxed networks induce high retraction force and good shape recovery. In Fig. 8 (d, e), when the filler content is over 15wt%, R_f keeps constant and R_r decreases. This is due to excess MFC-BR (not incorporated in the PPC chain) would aggravate particle distribution and disturb chain motions, impeding the elastic properties of the material. Both strength and toughness must be considered to understand the shape memory behavior.[10, 40] Therefore, to achieve the best shape memory property, the content of MFC in PPC matrix should be controlled, which is the best at definite range of compound ratio due to increasing constraint of the micro-Brownian thermal motions of PPC chains.[12]

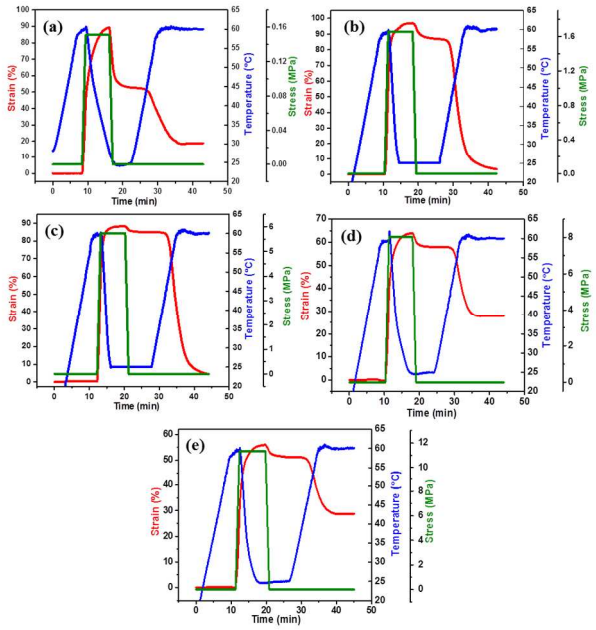

Fig. 8 The thermal-mechanical tensile curves of neat PPC and PPC/MFC-BR composites, (a)PPC, (b)PPC5, (c)PPC10, (d)PPC15, (e)PPC20.

Table. 2 Shape fix ratio (R_f) and recovery ratio (R_r) of neat PPC and PPC/MFC-BR composites.[a]

Sample	R_{f1} (%)	R_{r1} (%)	R_{f2} (%)	R_{r2} (%)	R_{f3} (%)	R_{r3} (%)
PPC	49.5	77.8	51.7	79.2	50.3	79.5
PPC5	90.3	94.9	91.3	94.6	91.5	94.3
PPC10	96.6	94.3	95.8	94.1	95.6	93.9
PPC15	92.2	57.9	92.4	57.5	92.8	58.6
PPC20	93.6	44.5	93.5	45.7	94.4	46.2

[a] R_{fx}, R_{rx}: strain recovery values for the x circle.

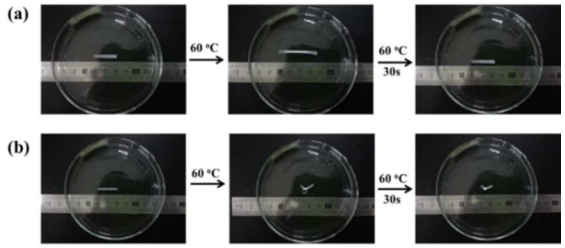

Fig. 9 An example for the recovery process of shape memory effect when the PPC5 sample was placed in oven 60 °C. (a) a stretched strip; (b) a knot was made with the stretched strip.

3.8 Self-healing behavior

In the following, optical images and tensile tests were used to investigate the shape memory assisted self-healing behavior of PPC composites. As shown in Fig. 10, it's found that the incorporation of MFC-BR significantly improves the scratch resistance of PPC. For pure PPC, large crack is developed along the scratch direction. Under identical scratching conditions, a narrower scratch is formed in PPC5 and PPC10, indicating MFC-BR enhances the fracture strength. There is still a noticeable scratch for pure PPC at 60 °C. For PPC5 and PPC10, the scratch is almost gone when heated to 60 °C. The result indicates that the contraction of PPC5 and PPC10 during the heating in the direction perpendicular to the scratch favors the closure of the scratch and the following self-healing by molecular interdiffusion.[19, 21] However, for PPC20, although the scratch is narrower than PPC, PPC5 and PPC10, the decreased elasticity hinders the scratch closure and the following self-healing at 60°C, which is consistent with the above results (e.g, the results from SEM, DMA and shape memory experiment). It can be concluded that with the assistance of SME and the reinforcement of

MFC-BR fibers, the polymer composites show improved scratch resistance and scratch self-healing behavior.

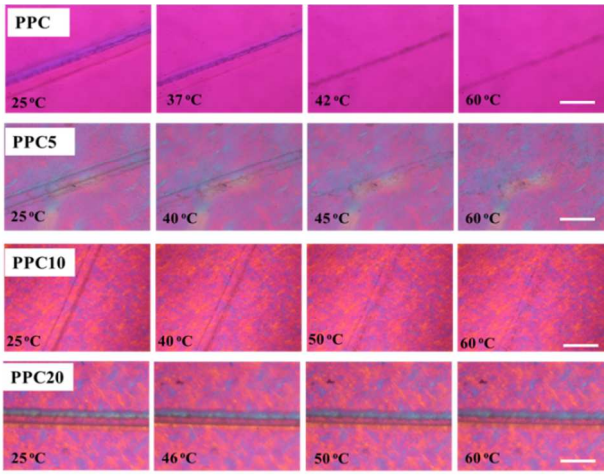

Fig. 10 POM images showing the evolution of the scratch on the surface of PPC and PPC/MFC-BR composites. Scale bar is 200 μm.

In addition to the healing of morphology, the recovery of elongation is also a key factor for evaluating the healing efficiency. The stress-strain curves of neat, scratched, and healed samples with or without previous stretching (PPC, PPC5) are given in Fig. 11. Here, it should be noted that due to different test instruments and conditions, there is much difference between the results in Fig. 5a and Fig. 11. Due to the scratch on the surface, the elongation of PPC is greatly decreased from 300% to 40% while it is 130% for a healed sample, which demonstrates that over 40% lost elongation is recovered after healing. By comparison, the elongation of PPC5 recovers almost completely. The reverse plasticity shape memory effect lies in the material's capability to recover scratch defects upon thermal activation.[22] Indeed, upon heating to 60 °C, the scratch of PPC5 is almost gone because of the improved scratch resistance and resilience to scratch formation. However, the crack width of pure PPC do become smaller but the damage is not healed completely, due to the relatively low shape recovery ratio and more material removal by the sharp blade. To confirm shape memory assisted self-healing effect, control tensile test experiment with scratch but without pre-stretching was also carried out. As shown in Fig. 11, the elongation of PPC and PPC5 composites without previous stretching cannot fully recover after heating to 60 °C. Clearly, shape memory

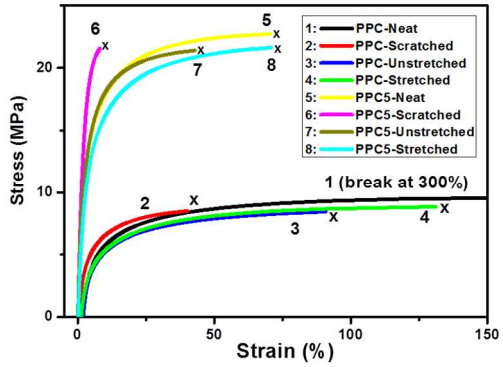

Fig. 11 Stress-strain curve for representative neat, scratched, and healed samples of PPC, PPC5.

behavior can be used to aid the healing process by bringing fractured surfaces into close proximity, allowing them to be more efficiently healed.

In this study, we have demonstrated that MFC-BR could enhance the shape memory property of PPC and PPC/MFC-BR composites present the self-healing ability when the content of MFC-BR is 5% and 10%. Herein, to give a vivid description of the shape recovery and self-healing behavior of PPC/MFC-BR composites, two sketches are drawn according to the above discussions (Fig. 12). Thus, we presume that the properties of PPC/MFC-BR could be explained as follows. First, PPC itself has poor shape memory ability. Therefore, MFC-BR plays a dominant role in improving the shape memory property of PPC. The result is ascribed to the high surface area of MFC-BR that could react with a large amount of PPC molecules and generate sufficient interfacial interactions, which could control the motion of PPC chains. Therefore, the mobility of PPC chain segments is responsible for holding the temporary shape and nonreversible cross-linkers (MFC-BR fibers) determine the permanent shape**.** Second, self-healing generally involves the closure of scratch, the diffusion of the polymer chain segments across the wounded interfaces and rearrangement to heal the scratches above Tg. In our work, the closure of scratch and the mobility of PPC chain segments are the key factors to realize self-healing behavior. We note that the composites (PPC5, PPC10) display significant property enhancement over the unfilled PPC including shape memory property, scratch resistance and thermal healing capability.

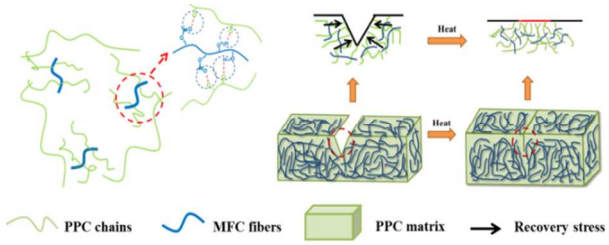

Fig. 12 Schematic illustration of the interactions between PPC with MFC fibers and the shape memory assisted self-healing concept.

4 Conclusions

A novel biological friendly SMP based on PPC and MFC-BR has been prepared. By using a chemical-co-physical approach, a high content of MFC-BR was incorporated into PPC up to 20wt% with excellent dispersion. The high content fillers could form a network structure in the PPC matrix. XPS indicated that strong interfacial interaction between PPC and MFC-BR could exist in the composites. The existence of MFC-BR not only could significantly enhance mechanical strength of PPC both at room temperature and high temperature (above the Tg of PPC), but also improved the shape memory property of PPC at definite content (5~10 wt%). Moreover, with the assistance of shape memory effect and the reinforcement of MFC-BR fibers, the polymer composites also showed scratch resistance and scratch self-healing behavior. Our work provides a composite approach to tune the shape memory behaviors of polymers and may contribute to the application of PPC in smart materials field.

Acknowledgements

We would like to express our sincere thanks to the National Natural Science Foundation of China for financial support (Grant No. 50903048, 51121001 and 21404075).

Notes and references

[a] College of Polymer Science and Engineering, State Key Laboratory of Polymer Materials Engineering, Sichuan University, Chengdu 610065, China. Tel/Fax: +86-28-8546-1759. E-mail: qiangfu@scu.edu.cn.

[b] Department of Chemical and Materials Engineering, Chang Gung University, Tao-Yuan 333, Taiwan. Tel.: +886 3 2118800x5297; fax: +886 3 2118668. E-mail: maxson@mail.cgu.edu.tw.

† Footnotes should appear here. These might include comments relevant to but not central to the matter under discussion, limited experimental and spectral data, and crystallographic data.

Electronic Supplementary Information (ESI) available: [details of any supplementary information available should be included here]. See DOI: 10.1039/b000000x/

1. A. Lendlein and S. Kelch, *Angew. Chem., Int. Ed., 2002,* **41***, 2034.*
2. C. Liu, H. Qin and P. T. Mather, *J. Mater. Chem.*, 2007, **17**, 1543.
3. Y. Yang and M. W. Urban, *Chem. Soc. Rev.,* 2013, **42**, 7446.
4. X. Qi, X. Yao, S. Deng, T. Zhou and Q. Fu, *J. Mater. Chem. A*, 2014, **2**, 2240.
5. W. Wang, H. Lu, Y. Liu and J. Leng, *J. Mater. Chem. A*, 2014, **2**, 5441.
6. H. Meng and G. Li, *J. Mater. Chem. A*, 2013, **1**, 7838.
7. J. Hu, Y. Zhu, H. Huang and J. Lu, *Prog. Polym. Sci.,* 2012, **37**, 1720.
8. P. Miaudet, A. Derre, M. Maugey, C. Zakri, P. M. Piccione, R. Inoubli and P. Poulin, *Science*, 2007, **318**, 1294.
9. L. Viry, C. Mercader, P. Miaudet, C. Zakri, A. Derré, A. Kuhn, M. Maugey and P. Poulin, *J. Mater. Chem.*, 2010, **20**, 3487.
10. J. Dong, J. Ding, J. Weng and L. Dai, *Macromol. Rapid. Commun.,* 2013, **34**, 659.
11. X. Zheng, S. Zhou, X. Li and J. Weng, *Biomaterials*, 2006, **27**, 4288.
12. S. B. Zhou, X. T. Zheng, X. J. Yu, J. X. Wang, J. Weng, X. H. Li, B. Feng and M. Yin, *Chem. Mater.*, 2007, **19**, 247.
13. K. Du and Z. Gan, *J. Mater. Chem. B*, 2014, **2**, 3340.
14. J. Xu and J. Song, *Proc. Natl. Acad. Sci. U. S. A., 2010, **107**, 7652.*
15. P. Agarwal, M. Chopra and L. A. Archer, *Angew. Chem., Int. Ed.,* 2011, **50**, 8670.
16. F. Cao and S. C. Jana, *Polymer*, 2007, **48**, 3790.
17. Y. Zhang, Q. Wang, C. Wang and T. Wang, *J. Mater. Chem.*, 2011, **21**, 9073.
18. B. T. Michal, C. A. Jaye, E. J. Spencer and S. J. Rowan, *ACS Macro Lett.*, 2013, **2**, 694.
19. X. Wang, J. Zhao, M. Chen, L. Ma, X. Zhao, Z. M. Dang and Z. Wang, *J. Phys. Chem. B,* 2013, **117**, 1467.
20. X. Luo and P. T. Mather, *ACS Macro Lett.*, 2013, **2**, 152.
21. Y. Bai, Y. Chen, Q. Wang and T. Wang, *J. Mater. Chem. A*, 2014, **2**, 9169.
22. X. Xiao, T. Xie and Y. T. Cheng, *J. Mater. Chem.*, 2010, **20**, 3508.
23. Y. K. Bai, Q. H. Wang and T. M. Wang, *Carbohydr. Polym.,* 2014, **104**, 101.
24. X. Hu, C. Xu, J. Gao, G. Yang, C. Geng, F. Chen and Q. Fu, *Compos. Sci. Technol.*, 2013, **78**, 63.
25. G. Yang, C. Geng, J. Su, W. Yao, Q. Zhang and Q. Fu, *Compos. Sci. Technol.*, 2013, **87**, 196.
26. J. Gao, F. Chen, K. Wang, H. Deng, Q. Zhang, H. Bai and Q. Fu, *J. Mater. Chem.*, 2011, **21**, 17627.
27. X. Shi and Z. Gan, *Eur. Polym. J.*, 2007, **43**, 4852.
28. Z. Zhang, J. H. Lee, S. H. Lee, S. B. Heo and C. U. Pittman, *Polymer*, 2008, **49**, 2947.
29. X. Yao, X. Qi, Y. He, D. Tan, F. Chen and Q. Fu, *ACS. Appl. Mater. Interfaces*, 2014, **6**, 2497.
30. I. Siro and D. Plackett, *Cellulose*, 2010, **17**, 459.
31. J. Lu, P. Askeland and L. T. Drzal, *Polymer*, 2008, **49**, 1285.
32. P. Huang, M. Wu, S. Kuga, D. Wang, D. Wu and Y. Huang, *ChemSusChem*, 2012, **5**, 2319.
33. J. Gao, H. Bai, X. Zhou, G. Yang, C. Xu, Q. Zhang, F. Chen and Q. Fu, *Nanotechnology*, 2014, **25**, 025702.
34. D. F. Wu, Y. S. Zhang, M. Zhang and W. Yu, *Biomacromolecules*, 2009, **10**, 417.
35. I. S. Gunes, C. Pérez-Bolivar, F. Cao, G. A. Jimenez, P. Anzenbacher and S. C. Jana, *J. Mater. Chem.*, 2010, **20**, 3467.
36. Z. Tang, D. Sun, D. Yang, B. Guo, L. Zhang and D. Jia, *Compos. Sci. Technol.*, 2013, **75**, 15.
37. S. Bayar, F. Delale and B. M. Liaw, *J. Aerosp. Eng.*, 2014, **27**, 491.
38. A. Lovdal, L. L. Laursen, T. L. Andersen, B. Madsen and L. P. Mikkelsen, *J. Appl. Polym. Sci.,* 2013, **128**, 2038.
39. D. H. Jung, H. M. Jeong and B. K. Kim, *J. Mater. Chem.*, 2010, **20**, 3458.
40. H. Luo, J. Hu and Y. Zhu, *Mater. Lett.*, 2011, **65**, 3583.

